In vitro modeling of the microvascular occlusion and thrombosis that occur in hematologic diseases using microfluidic technology

Michelle Tsai,[1,2,3] Ashley Kita,[1,2,3] Joseph Leach,[4] Ross Rounsevell,[1] James N. Huang,[5] Joel Moake,[6] Russell E. Ware,[7] Daniel A. Fletcher,[1,8] and Wilbur A. Lam[2,3,9,10]

[1]Department of Bioengineering, University of California, Berkeley, California, USA. [2]Department of Pediatrics, Division of Pediatric Hematology/Oncology, Aflac Cancer Center and Blood Disorders Service of Children's Healthcare of Atlanta, Emory University School of Medicine, Atlanta, Georgia, USA. [3]Wallace H. Coulter Department of Biomedical Engineering, Georgia Institute of Technology and Emory University, Atlanta, Georgia, USA. [4]UCSF School of Medicine, San Francisco, California, USA. [5]Department of Pediatrics, Division of Pediatric Hematology/Oncology, UCSF, San Francisco, California, USA. [6]Department of Bioengineering, Rice University, Houston, Texas, USA. [7]International Hematology Center of Excellence, Department of Pediatrics, Baylor College of Medicine, Houston, Texas, USA. [8]Graduate Group in Biophysics, University of California, Berkeley, California, USA. [9]Center for Endothelial Cell Biology, Children's Healthcare of Atlanta, Atlanta, Georgia, USA. [10]Winship Cancer Institute of Emory University, Atlanta, Georgia, USA.

In hematologic diseases, such as sickle cell disease (SCD) and hemolytic uremic syndrome (HUS), pathological biophysical interactions among blood cells, endothelial cells, and soluble factors lead to microvascular occlusion and thrombosis. Here, we report an in vitro "endothelialized" microfluidic microvasculature model that recapitulates and integrates this ensemble of pathophysiological processes. Under controlled flow conditions, the model enabled quantitative investigation of how biophysical alterations in hematologic disease collectively lead to microvascular occlusion and thrombosis. Using blood samples from patients with SCD, we investigated how the drug hydroxyurea quantitatively affects microvascular obstruction in SCD, an unresolved issue pivotal to understanding its clinical efficacy in such patients. In addition, we demonstrated that our microsystem can function as an in vitro model of HUS and showed that shear stress influences microvascular thrombosis/obstruction and the efficacy of the drug eptifibatide, which decreases platelet aggregation, in the context of HUS. These experiments establish the versatility and clinical relevance of our microvasculature-on-a-chip model as a biophysical assay of hematologic pathophysiology as well as a drug discovery platform.

Introduction

Hematologic diseases often involve pathological biophysical interactions among blood cells, endothelial cells, and soluble factors (e.g., cytokines, coagulation factors, etc.) that lead to microvascular occlusion and thrombosis, such as in sickle cell disease (SCD) and thrombotic microangiopathies (1–3). Alterations in the biophysical properties, such as cell adhesion, cell aggregation, and cell deformability, of blood cells contribute to the pathophysiology of these disease states, ultimately leading to compromise of microvascular flow in vital organs (4, 5). Although animal models have vastly improved our understanding of these diseases, complementary in vitro systems have the potential to offer valuable quantitative insights into how biophysical properties influence pathophysiology.

Most biophysical studies have primarily employed in vitro methods that focus on a singular, isolated aspect of microvascular occlusion and thrombosis. For example, techniques that quantify cell deformability, such as micropipette aspiration and atomic force microscopy, have been broadly applied (6). Similarly, parallel plate flow chambers have been used extensively to study the adhesion dynamics between blood cells and cultured endothelial cell monolayers and have led to important advances in our understanding of vascular and hematologic pathology (7). Furthermore, aggregation assays have extended to clinical use to study platelet function (8). However, no existing in vitro assays effectively integrate these pathological processes within a single system to enable the quantitative investigation of microvascular occlusion in hematologic diseases.

In the past decade, advances in microfabrication technologies have provided useful, inexpensive, and easily reproducible microfluidic platforms for conducting microscale biological and biochemical experiments (9, 10). The ability to easily and tightly control biological conditions and the dynamic fluidic environment within the system enable microfluidics to be ideal tools for quantitatively analyzing hematologic and microvascular processes (11–13). Accordingly, researchers have recently applied microfluidic devices to study blood cell deformability, blood flow, and blood–endothelial cell interactions (14–17). Some reports have described successful cross-sectional coverage of endothelial cells in microfluidic systems (18, 19), but these devices were larger than the microvascular size scale relevant to the pathologic processes at that anatomic level. Therefore, a system that accurately recapitulates the cellular, physical, and hemodynamic environment of the microcirculation is needed to improve our understanding of microvascular diseases. No published reports to date have applied patient blood samples in "endothelialized" microfluidic systems at the microvascular size scale (<50 μm).

To that end, we have developed a simple, single-mask microfabrication process combined with standard endothelial cell

Authorship note: Michelle Tsai and Ashley Kita contributed equally to this work.
Conflict of interest: The authors have declared that no conflict of interest exists.
Citation for this article: *J Clin Invest.* 2012;122(1):408–418. doi:10.1172/JCI58753.

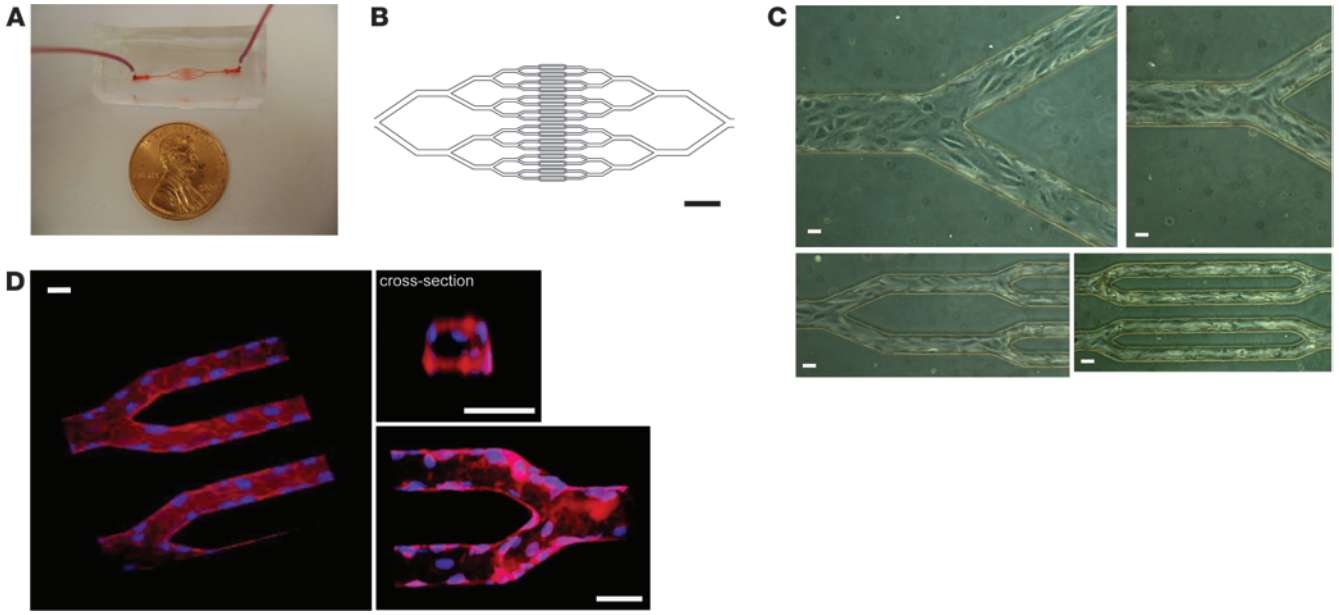

Figure 1
An in vitro microfluidic model of the microvasculature for investigating disease processes involving biophysical cellular interactions. (**A**) Macroscopic view of PDMS microdevice. (**B**) Software-generated image used to develop the photolithography mask that defines the geometric pattern of the microfluidic channels. Smallest channels in this pattern are 30 μm wide. Scale bar: 600 μm. (**C**) Brightfield images show that within 48 hours, HUVECs seeded into the microdevice are cultured to confluency. Images are taken from different areas of the same device at the same scale. Scale bars: 30 μm. (**D**) 3D renderings of multiple confocal microscopy using fluorescent cell membrane (red) and cell nuclear (blue) dyes show that the endothelial cells line the entire inner surface of the microfluidic channels. The cross-sectional view also reveals that the cells round off the square corners of the smallest microchannels. Scale bars: 30 μm.

culture techniques to fabricate a microvascular-sized fluidic system that incorporates a confluently cultured endothelial cell monolayer that covers the entire 3D inner surface of the microfluidic system. Our microsystem fully integrates blood–endothelial cell adhesion, cellular aggregation, cellular mechanical properties (i.e., size, deformability, etc.), microvascular geometry, and hemodynamics and is therefore suitable for quantitative biophysical analyses of diseases involving microvascular occlusion and thrombosis. This endothelialized in vitro model of the microvasculature is ideal for studying hematologic diseases with pathologies that span the fields of both biology and biophysics, such as sepsis/inflammatory disorders, SCD, and thrombotic microangiopathies. Here, we show that our microfluidic system is capable of identifying specific pathophysiological characteristics related to the interactions between blood cells and endothelial cells combined with geometric and flow constraints of microvasculature. Specifically, we found that (a) in the context of inflammation, TNF-α activation of both leukocytes and endothelial cells leads to a much higher rate of microchannel obstruction than activation of endothelial cells alone, (b) the multiple effects of hydroxyurea lead to an overall increase in microvascular flow using sickle cell blood, and (c) with shiga toxin (STX) activation, our microsystem functions as an in vitro model of hemolytic uremic syndrome (HUS), a thrombotic microangiopathy. Our results demonstrate that the endothelialized in vitro microsystem is capable of capturing specific biophysical interactions involved in these and other diseases, and it holds promise as a drug discovery platform for hematologic diseases involving the microvasculature.

Results

Fabrication of the microvasculature on a chip. Using standard microfabrication techniques and an endothelial cell seeding/culture protocol, we developed a process to create systems of 3D microvascular-sized fluidic channels that are completely lined with endothelial cell monolayers. The micropatterned fabricated silicon master functions as a mold, and the microchannels are cast in polydimethylsiloxane (PDMS), a silicone elastomer (Figure 1A). This allows multiple, identical, and disposable microfluidic devices to be made from the same master and enables the process to be reproducible and inexpensive.

Microfluidic networks of branching microchannels were fabricated with a standard single-mask photolithography process based on our previous design (14), with the smallest channels at 30 μm in width and height within the microvascular size scale (Figure 1B). The 30-μm microchannel size was chosen to model postcapillary venules and arterioles, which are approximately the same size in diameter. Using a standard syringe pump, we seeded the microfluidic chips with human endothelial cells under our optimized conditions. Confluent monolayers developed within 24 to 48 hours, as the cells were exposed to a constant flow of culture medium within the microfluidic system. Figure 1C shows brightfield microscopy images of different areas of the same network in the same device in which HUVECs successfully seed the entire microfluidic system within 36 hours. Live cell confocal imaging using fluorescent cell membrane and cell nuclei dyes (see Methods) revealed that HUVECs appeared to successfully culture the entire 3D inner surface of the microfluidic system to confluence (Figure 1D and Supplemental Videos 1 and 2; supplemental material available online with this article; doi:10.1172/JCI58753DS1). The

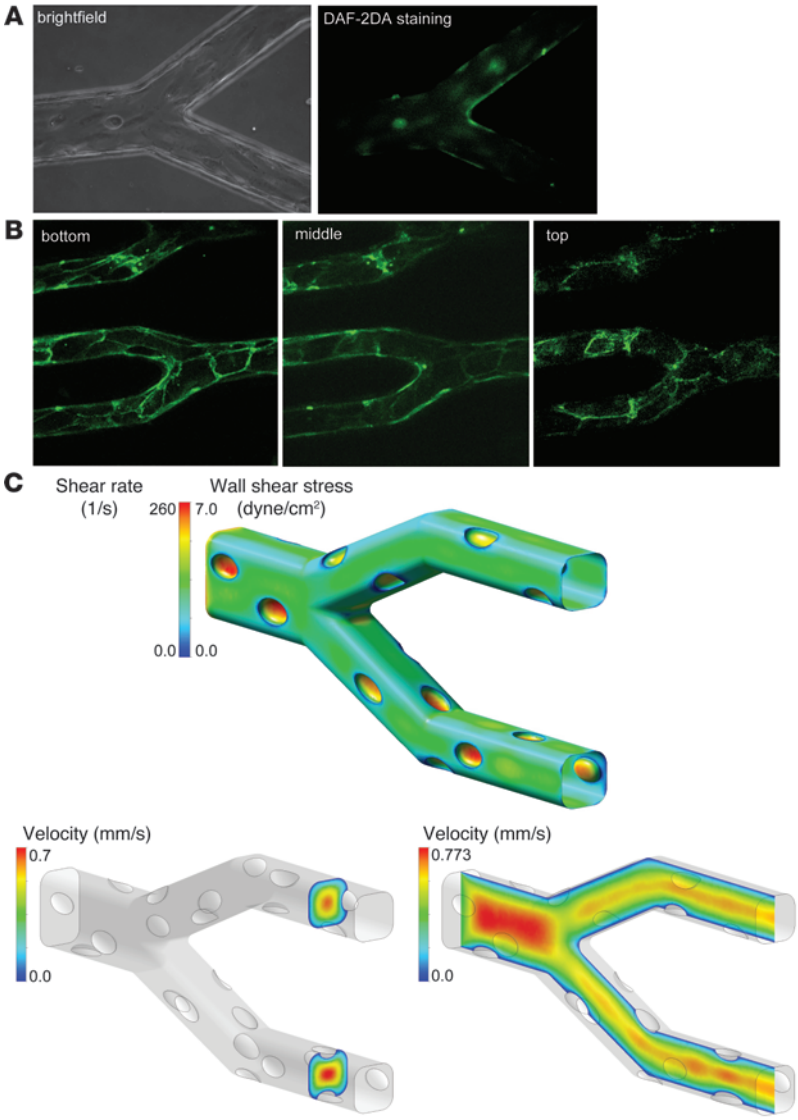

Figure 2
Characterization of the "endothelialized" microvasculature on a chip. (**A**) Epifluorescence microscopy (with corresponding brightfield image) shows that HUVECs cultured in the microfluidic device stain positively with DAF-2DA, providing evidence that the endothelial cells are functional and appropriately produce NO. (**B**) Endothelial cell junctions also appropriately stain positive for anti–VE-cadherin–FITC. (**C**) Computational fluid dynamic modeling revealed that at centerline flow velocities and viscosities representative of physiologic microvascular conditions, flow was highly organized and that wall shear stress/shear rate levels were at physiological levels. For this particular simulation, the centerline velocity was adjusted to be 0.7 mm/s and viscosity was specified at 2.7 cP, corresponding to in vivo conditions in postcapillary venules of approximately 30 μm in diameter.

presence of endothelial cells decreased the effective lumen size to a range of 24 to 28 μm in width/height for the smallest microchannels, and their cell bodies yielded a more rounded cross-section of the microchannels (Figure 1D), enabling conditions to be more physiologic. Similar results were seen with other human endothelial cells, including those of microvascular origin, such as human lung microvascular endothelial cells (HLMVECs; Supplemental Figure 1) and human microvascular endothelial cell line 1 (HMEC-1).

As further confirmation of their viability, endothelial cells cultured within the microfluidic system appropriately expressed NO and VE-cadherin, as measured with 4,5-diaminofluorescein diacetate (DAF-2DA) fluorescence and immunofluorescence, respectively (Figure 2, A and B). Expression of NO is an integral part of endothelial function and requires the cells to be viable and functional (20, 21). Similarly, VE-cadherin expression occurred at endothelial cell junctions and was present throughout the entire inner surface in our endothelialized microdevices, providing further evidence the endothelial cells grossly achieve confluence in our system and are functioning appropriately (22). Together, these experiments showed that the cells are viable in the microfluidic system and appropriately exhibit behavior similar to those in 2D cell-culture conditions.

Fluid dynamic modeling of the "endothelialized" microvasculature on a chip. To investigate the fluidic environment of the smallest channels in the fabricated networks, we performed computational fluid dynamics (CFD) analyses on the geometry of the microchannels observed under microscopy. Additional fluid-structure interaction (FSI) analyses were made to explore effects resulting from the physical structure and deformation properties of the endothelial cell bodies and nuclei (see Methods). Simulations of steady-state flow in the endothelialized channels were conducted using a range of centerline flow velocities (0.1 mm/s to 7 mm/s) representative of physiologic microvascular conditions. A range of viscosities (2.0 to 4.0 centipoise [cP]) was specified to explore flow characteristics in blood with varying hematocrit and different maximum shear rates. As our model is intended to give an approximate picture of the average shear experienced by the endothelial cells, we chose the viscosity range to coincide with apparent viscosities determined from in vivo experimental observation (23). The Reynolds number (Re) is a dimensionless number representing the ratio of inertial and viscous forces experienced by the fluid in a flow system and is commonly used as a metric to describe the fluid's tendency toward either well-organized or turbulent flow characteristics; in steady pipe flow, a Re of less than approximately 2000 is generally regarded as resulting in organized, laminar flow. In the Stokes flow regime (Re << 1) of our system, flow was highly organized and displayed no inertia-driven features, such as recirculation zones following cellular protrusions into the channel at nuclear locations. Flow shear stresses calculated at the endothelial surface were consistent with those reported in the literature for similarly sized vessels in vivo (Figure 2C) (4, 24, 25). Increasing the flow velocity within the physiologic range increased the scale of the wall shear stresses, but the actual shear pattern remained nearly unchanged. Additionally, because the flow field remained viscosity-dominated, the flow patterns remained largely the same over the range of conditions explored.

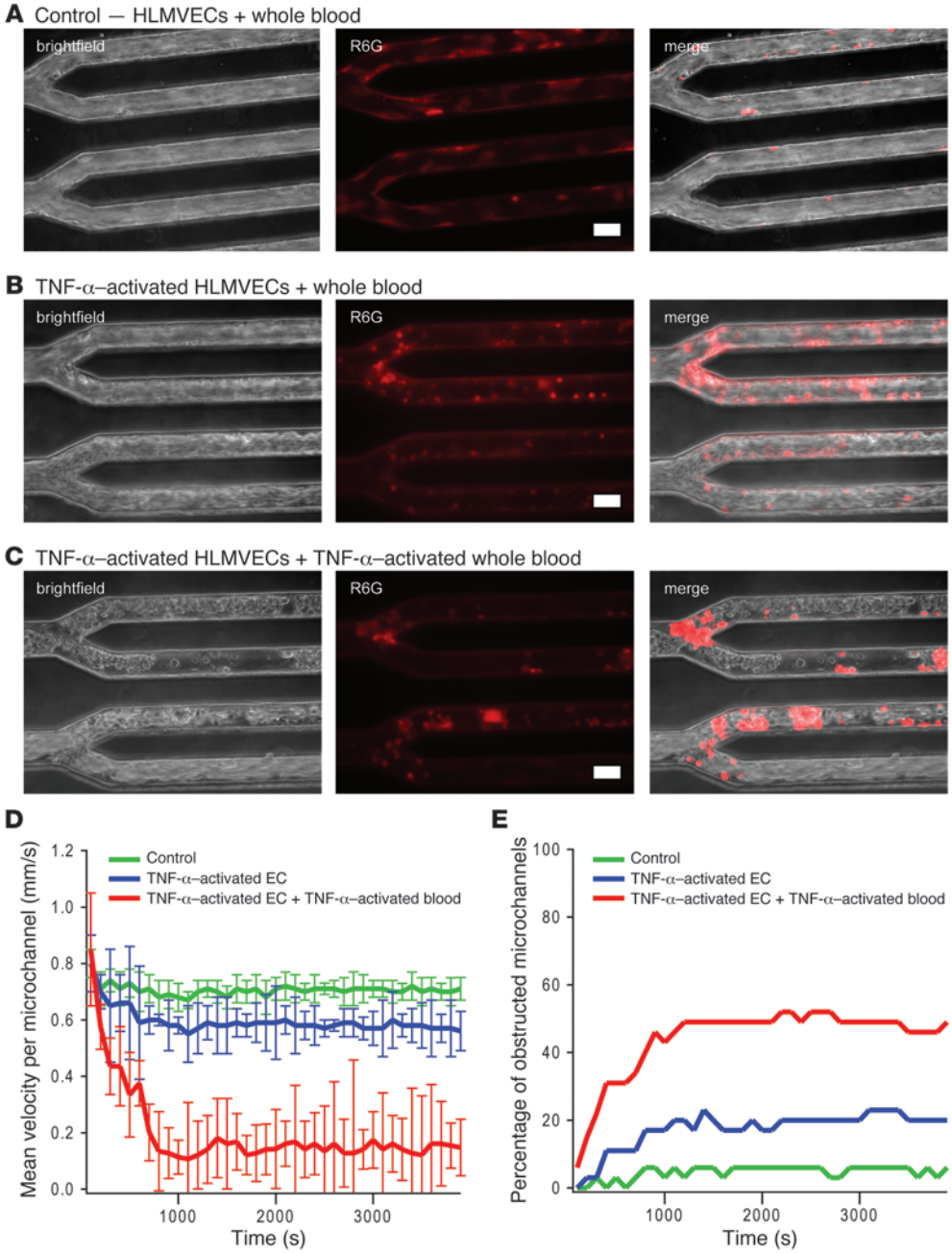

Figure 3

Decreased flow and microchannel occlusion due to activation with the inflammatory cytokine TNF-α. (**A**) Brightfield imaging and epifluorescence using R6G, a fluorescent dye that preferentially stains leukocytes and platelets, revealed that when whole blood is flowed into the microdevice cultured with HLMVECs at postcapillary venular flow conditions, flow is steady overall, with occasional rolling but few adherent leukocytes. (**B**) When endothelial cells were activated with TNF-α before whole blood was flowed into the system, brightfield and R6G staining revealed a slight decrease in overall flow velocity, with occasional microchannel obstructions as well as an increase in adherent leukocytes. (**C**) TNF-α activation of both the endothelial cells and whole blood revealed a dramatic increase in microchannel obstruction, with subsequent decrease in overall flow likely due to a combination of increased adhesion and cell stiffness. Scale bars: 30 μm. (**D**) The addition of 0.5 μm fluorescent beads mixed into the whole blood samples enabled velocity quantification in each microchannel. The centerline bead velocity was measured for each channel and averaged for each data point. Compared with the control condition (no TNF-α activation), the average centerline velocity per microchannel (n = 32 microchannels/device) was significantly decreased when endothelial cells were preactivated with TNF-α ($P < 0.05$) and even more so when both endothelial cells and whole blood were preincubated with TNF-α ($P < 0.005$). Error bars show SD. (**E**) The percentage of microchannels completely obstructed due to aggregates of leukocytes increased with TNF-α of endothelial cells and increased even further with TNF-α activation of both the endothelial cells and whole blood.

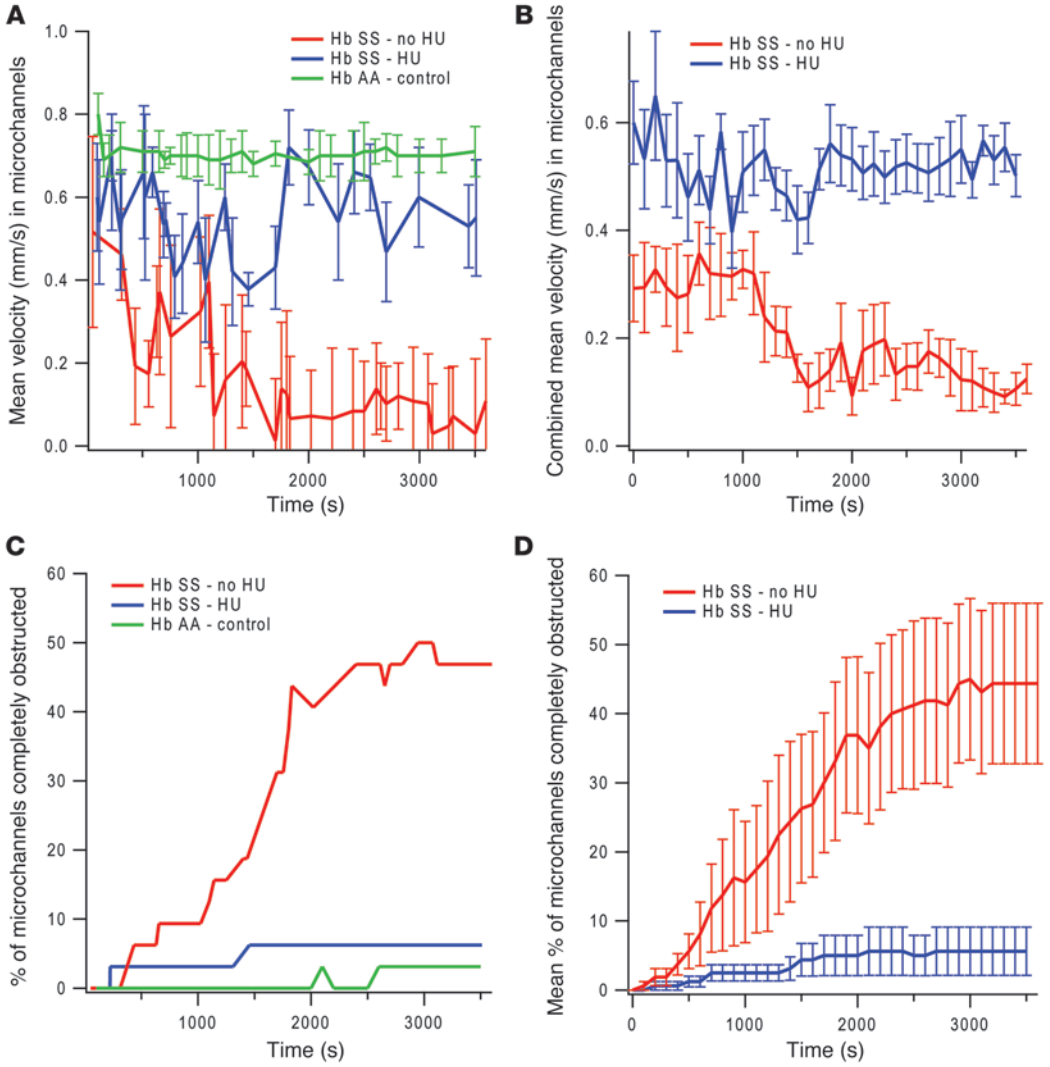

Figure 4

Application of the microvasculature on a chip to vasoocclusion in SCD. (**A**) Under identical initial hemodynamic conditions comparable to postcapillary venules using a microdevice cultured with HLMVECs, the microchannel velocity ($n = 32$ microchannels/device) of a whole blood sample taken from a healthy volunteer was compared with that of a whole blood sample taken from an SCD patient treated with HU and a whole blood sample from an SCD patient not treated with HU. Flow patterns of both sickle cell samples were much less steady than that of the control sample, and velocities of the sickle cell samples were lower than that of the control. Within 20 minutes of the start of the experiment until the end of the experiment, the velocity of the sickle cell HU^- sample was consistently lower than that of the sickle cell HU^+ sample ($P < 0.03$). (**B**) These differences became more apparent when the average of velocity curves of blood samples taken from 5 different HU^+ sickle cell blood samples were compared with the average of velocity curves of 5 different HU^- sickle cell blood samples ($P < 0.008$). (**C**) Similarly, a sickle cell HU^- whole blood sample exhibited a higher rate of microchannel obstruction than a sickle cell HU^+ whole blood sample, and microchannel obstruction in the HU^- sample was even higher when compared with that of a healthy control. (**D**) Again, the differences became more apparent when the average of 5 obstruction curves from different HU^+ sickle cell blood samples was compared with the average of 5 HU^- sickle cell blood samples ($P < 0.032$). All SCD patients in this study had hemoglobin SS (Hb SS), whereas health controls had hemoglobin AA (Hb AA). All error bars represent SD.

The results of these simulations and their variation over an appropriate range of boundary conditions support our in vitro microvasculature model as a reasonable and accurate approximation of the microcirculatory flow conditions observed in vivo.

To test the initial predictions of our CFD analyses, normal whole blood mixed with fluorescent 0.5-μm beads used to track flow velocity was injected into the in vitro microvasculature model using a standard syringe pump. Using epifluorescence video microscopy to track flow in the 30-μm microchannels, we adjusted initial maximum bead velocity, V_{max}, which occurs at the center of the flow profile, to achieve the hemodynamic conditions of postcapillary venules in vivo with wall shear stresses ranging from 1 to 4 dyne/cm^2 (Figure 2C and refs. 4, 24, 26, 27). Epifluorescence and brightfield imaging revealed steady, highly organized flow free from stagnation zones or secondary, recirculation zones. This observation was expected, as turbulence should not occur in microfluidic devices (or microvascular flows) at low Re conditions, and was consistent with our fluid dynamic simulations (Figure 3, A and D, and Supplemental Video 3). The addition of 1 μg/ml of rhodamine 6G (R6G), a fluorescent marker that preferentially

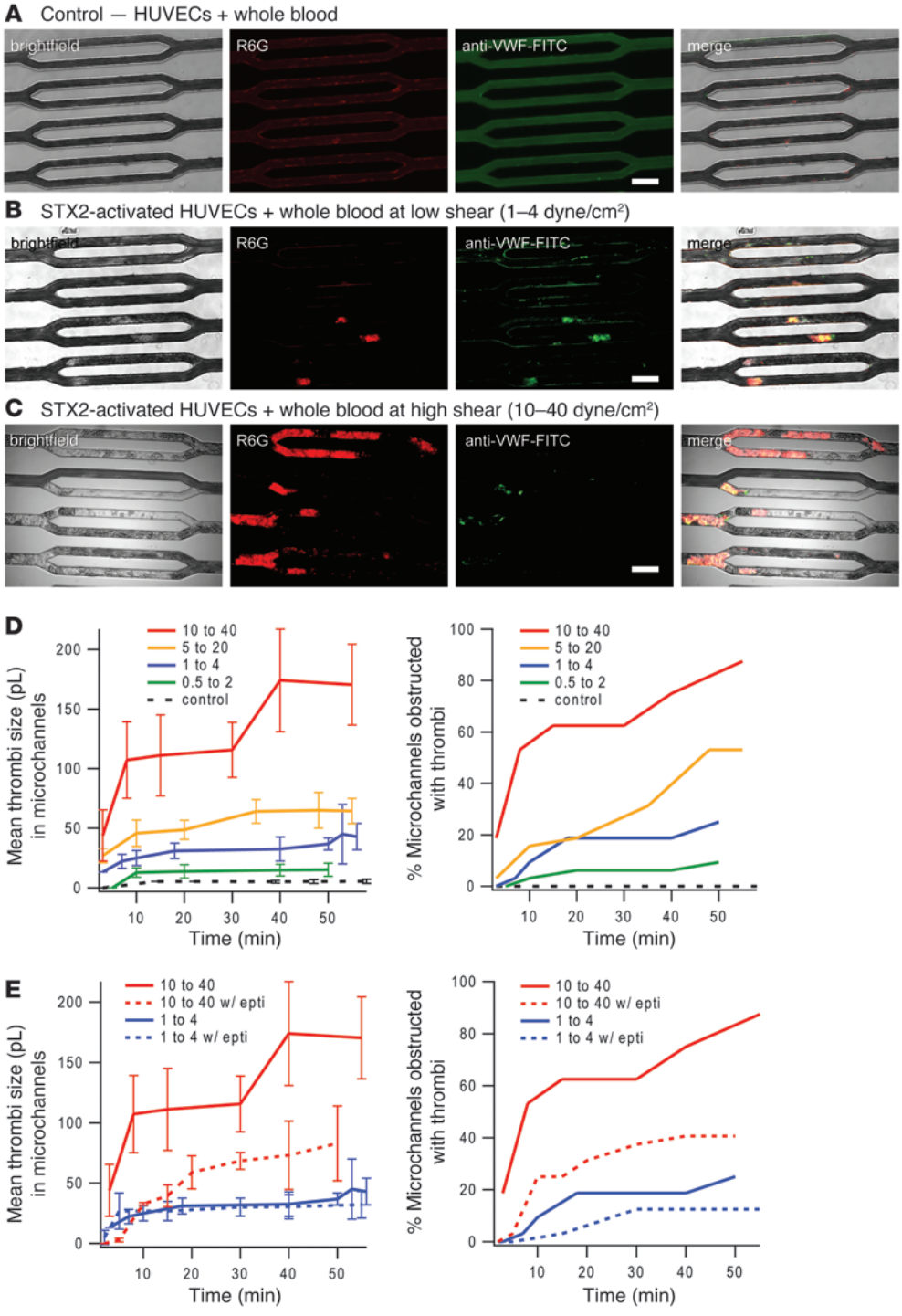

Figure 5
The microvasculature on a chip as an in vitro model for HUS. (**A**–**C**) HUVECs cultured to confluence in the microdevice were exposed to 30 pM STX2, a toxin that causes the hematologic manifestations of typical HUS, for 20 to 24 hours, and then whole blood containing STX2, R6G, and anti–vWF-FITC was flowed into the system at initial low shear (1–4 dyne/cm^2) and high shear stresses (10–40 dyne/cm^2). Compared with the control conditions (**A**), in which neither the endothelial cells nor whole blood was exposed to STX2, STX2 exposure led to the formation of thrombi consisting of leukocytes, platelets, and vWF, which occluded microchannels. This effect was more prominent at high shear (**C**) than low shear (**B**). (**D**) Multiple experiments using the same concentrations of STX2 were conducted at varying initial shear stress values. Thrombi volume (n = 32 microchannels/device), as measured using multiple confocal microscopy planes, and the percentage of microchannel occlusion due to STX2 exposure were shown to be shear dependent. (**E**) The addition of eptifibatide, a glycoprotein IIb/IIIa antagonist that inhibits platelet aggregation, in whole blood attenuated STX2-induced thrombi formation and microchannel obstruction. Interestingly, this effect was more pronounced at higher shear. All error bars represent SD. Scale bars: 80 μm.

stains leukocytes and platelets (28, 29), revealed occasional rolling, but no prolonged adhesion, of leukocytes and little microchannel obstruction (Figure 3, A and D, and Supplemental Video 4). Culturing the system with either HUVECs or HLMVECs showed no differences in flow patterns, leukocyte adhesion, or microchannel obstruction. These data experimentally confirm that our microfluidic system is a viable in vitro platform to study microcirculatory flow and cellular interactions and is compatible with different types of endothelial cells from different anatomic sites.

Activation with the inflammatory cytokine TNF-α leads to microchannel occlusion. Endothelial cell activation with the inflammatory cytokine TNF-α is known to upregulate expression of adhesion molecules such as VCAM-1 and ICAM-1 (30, 31). In pathologic disorders such as sepsis, excessive amounts of cytokines lead to dysregulated adhesion molecule expression in the microvascular endothelium of organs such as the lungs (32). To more appropriately model this process, we cultured HLMVECs in the microfluidic systems for these experiments. Confluent HLMVECs cultured in

the microdevice were incubated with 10 ng/ml of TNF-α in medium and then exposed to normal whole blood under the same initial hemodynamic conditions as in the control experiment without TNF-α exposure (described above). R6G staining revealed increased leukocyte adhesion as compared with the control (Figure 3B and Supplemental Video 5). In addition, brightfield imaging and fluorescent bead tracking revealed that increased leukocyte adhesion to endothelial cells leads to obstruction of a proportion of microchannels and overall decreased flow (Figure 3, B and D, and Supplemental Video 6). In sepsis, cytokines also activate, stiffen, and "prime" leukocytes, and this process is thought to contribute to microvascular occlusion and subsequent end-organ damage (33). Exposure of TNF-α–activated HLMVECs in our microfluidic system to TNF-α–activated leukocytes in whole blood led to a more than 7-fold increase in microchannel obstruction and an approximately 80% decrease in flow as compared with the control (Figure 3, C–E, and Supplemental Videos 7 and 8). Our observations therefore suggest that cytokine-mediated leukocyte activation and cytokine-mediated endothelial adhesion, both of which are well documented (30, 31), may have synergistic roles in the pathophysiology of inflammatory disorders such as sepsis. Furthermore, as data from our system provide a quantitative framework for studying microvascular occlusion, our microvasculature on a chip could enable researchers to quantitatively determine the relative contributions of leukocyte activation and endothelial cell adhesion toward this process. These proof-of-concept experiments highlight the system's capabilities of investigating pathologic processes that involve blood cells and the endothelium in different anatomic sites. In addition, these results also establish the microvasculature on a chip as a viable in vitro system to quantitatively study the biophysical aspects of sepsis and inflammatory disorders.

Application of the microvasculature on a chip to vasoocclusion in SCD. Vasoocclusion in SCD is inherently a biophysical process in which alterations in blood and endothelial cell mechanical properties, such as increased sickle red cell rigidity and upregulation of endothelial cell adhesion molecules, lead to profound pathologic effects on microvascular blood flow (2, 5). Previous research has primarily employed techniques such as micropipette aspiration and parallel plate flow chambers to characterize biophysical alterations in the cells involved in vasoocclusion, but only in isolation and separate from the other biophysical defects that occur (5, 11, 34–36). Although one elegant microfluidic study quantitatively characterizes the role of deoxygenation on sickle cell blood flow (10), no in vitro system has been reported that combines both the pathologic rheological aspects and the pathologic adhesion events that occur and interact in SCD. Our microvasculature on a chip is an ideal system to study the pathologic microvascular interactions that occur in sickle cell vasoocclusion.

A specific question that has arisen in the field of clinical hematology is what direct effect hydroxyurea, a drug now commonly used to prevent many of the complications of SCD (37), has on microvascular blood flow. Hydroxyurea is known to decrease the intracellular sickle hemoglobin polymerization rate within erythrocytes (38, 39), which leads to improved hydration and less rigidity of sickle red blood cells; decrease the expression of adhesion molecules and their subsequent adhesion to the endothelium (40); decrease the number of circulating leukocytes and reticulocytes that promote vasoocclusion (41); and promote NO release to improve vasodilatation (42), which collectively would decrease vascular occlusion and improve microcirculatory flow. On the other hand, hydroxyurea also increases the number of circulating red blood cells as well as their cellular volume (43), which could potentially increase the overall apparent microvascular viscosity and also the likelihood of microvascular obstruction (44). How these processes interact and collectively affect microvascular flow is not known and requires a system such as ours to improve our understanding of hydroxyurea-related hemodynamic effects in SCD.

To begin to address this question, we compared the flow characteristics of whole blood taken from SCD patients receiving hydroxyurea (HU^+) to those of whole blood from patients not receiving hydroxyurea (HU^-). To simulate physiologic conditions, the microfluidic system was cultured with endothelial cells from the pulmonary microvasculature, HLMVECs, as the pulmonary postcapillary venules are often the anatomic sites of SCD complications (41). Accordingly, the initial hemodynamic conditions were set to emulate those of postcapillary venules (30 μm microchannels, initial wall shear stress: 1–4 dynes/cm^2, initial V_{max}: ~1 mm/s). Control experiments with normal whole blood confirmed the presence of steady flow with no microchannel obstruction (Figure 4A). Under the same initial hemodynamic conditions, whole blood from all sickle patients, regardless of whether or not they were receiving HU, exhibited extremely uneven and unsteady flow, which is consistent with observations reported in the literature (Figure 4A and ref. 45). Although flow from sickle cell blood did not reach a steady state, after about 20 minutes, a distinct pattern occurred that distinguished blood from patients receiving HU from blood from patients not receiving the drug. HU^+ sickle cell blood achieved a higher average velocity than HU^- sickle cell blood, although neither approached the velocity and steady state of normal blood (Figure 4A shows examples of traces from 1 of each patient). The differences became more apparent when the average of velocity curves of blood samples taken from 5 different HU^+ sickle cell blood samples was compared with the average of velocity curves of 5 different HU^- sickle cell blood samples (Figure 4B). Even with this small sample size, the difference between final velocities of the 2 populations was statistically significant ($P < 0.008$). Furthermore, brightfield videomicroscopy revealed that, over the course of 30–60 minutes, HU^- sickle cell blood caused a greater degree of microchannel obstruction than HU^+ sickle cell blood (Figure 4C shows examples of traces from 1 of each patient type; Supplemental Videos 9 and 10). Similarly to what occurred in microchannel velocity, the differences became more apparent when the average of 5 obstruction curves from different HU^+ sickle cell blood samples was compared with the average of 5 HU^- sickle cell blood samples (Figure 4D), with a statistically significant difference ($P < 0.032$) between the final percentages of obstructed microchannels of each population.

Taken together, these initial observations support the notion that the decrease in red cell sickling, cellular adhesion, and leukocyte concentration induced by HU in SCD more than offsets and compensates for the general increase in red cell mass/hematocrit due to the drug. Of note, the experiments reported here were conducted under normoxic conditions, and further studies with our system will involve a quantitative assessment of how decreasing oxygen tension affects microchannel velocity and obstruction. Indeed, it is interesting that we observe such a dramatic effect without decreasing oxygen tension, which may suggest the effect of leukocytes and reticulocytes, both of which are known to have significant roles in initiating and promoting vasoocclusion (46).

The microvasculature on a chip as an in vitro model and drug discovery platform for HUS. Our system is also well suited for studying the underlying biophysical mechanisms of microvascular thrombosis, which occur in pathologic conditions such as thrombotic microangiopathies. A prototypical example of this type of disorder is the common, non–immune-mediated form of HUS. HUS is typically caused by a gastrointestinal infection with a STX-producing strain of *E. coli*, usually of the O157:H7 serotype, which subsequently leads to thrombosis and occlusion of the microvasculature in vital organs such as the kidney (47). STX causes direct dysfunction of the microvascular endothelium, leading to unregulated secretion of large multimers of vWF, platelet aggregation, and thrombi formation (3, 48). While the biological aspects of this process have been characterized, very little is known about biophysical aspects of this disease state, due in part to inadequate technology.

Previous work using parallel plate flow chambers showed that aggregates of leukocytes and platelets adhered to STX-exposed endothelial cells when heparinized whole blood was flowed over them (49). We sought to determine whether endothelial cell exposure to STX and whole blood would lead to thrombi-like aggregates capable of occluding our endothelialized microvasculature model and whether vWF secretion was involved in this process. HUVECs were cultured to confluence in our systems and then exposed to 30 pM of STX2, one of the isoforms of STX, for 20 to 24 hours. Heparinized whole blood containing 30 pM of STX2, R6G to fluorescently stain leukocytes and platelets, and anti–vWF-FITC was then flowed into the system, which was tracked with epi- and confocal fluorescence microscopy.

We observed that, indeed, thrombi consisting of leukocytes and platelets and involving vWF secretion formed within and occluded the endothelialized microchannels cultured with STX2-exposed endothelial cells, whereas the control conditions (no exposure to STX2) showed steady flow with no thrombi and minimal leukocytes adhering to the endothelialized channels (Figure 5, A, B, and D, and Supplemental Videos 11 and 12). Interestingly, as we varied the flow conditions over the range of physiologic microvascular shear stresses, we observed that as shear increased, thrombi size, the percentage of obstructed microchannels, and the rate of microchannel obstruction all increased (Figures 5, C and D, and Supplemental Videos 13 and 14). This suggests that thrombi formation and microvascular occlusion in HUS may be shear dependent, possibly due to shear activation of vWF (50). Similar results were obtained when the microfluidic system was cultured with HMEC-1 cells, but the differences between the control and experimental conditions were not as pronounced, likely because the decreased contact inhibition of HMEC-1 led to some microchannel obstruction in the control conditions.

As white blood cell counts correlate with poor clinical outcomes in HUS (51, 52), we sought to determine what specific leukocyte subpopulations were involved in thrombi formation and microchannel occlusion in our system. Exposure of whole blood containing anti–CD15-FITC antibody to detect neutrophils and anti–CD14-PE antibody to detect monocytes to STX-activated HUVECs in our microdevice revealed that both types of leukocytes were involved with thrombi formation, with more neutrophils present than monocytes (Supplemental Figure 2). This experiment demonstrates how our in vitro microvasculature model can easily accommodate live cell immunofluorescence microscopy to investigate the underlying mechanisms of microvascular interactions.

Finally, we found that the addition of an eptifibatide (final concentration: 2.4 μM), a glycoprotein IIb/IIIa antagonist that inhibits platelet aggregation (53), in whole blood attenuated STX2-induced thrombi formation and microchannel obstruction (Figure 5E). Interestingly, this effect was more pronounced at higher shear. Taken together, these observations suggest that platelet aggregation may have a significant role in HUS and that further clinical evaluation of medications such as eptifibatide as a HUS treatment or prophylactic may be warranted. Ongoing studies in our laboratory and others are addressing these issues.

Discussion

Here we describe the development and characterization of a new microfluidic device that recapitulates key aspects of the microvasculature that include size scale, an endothelial monolayer cultured throughout the entire 3D inner surface of the system, and physiologically relevant hemodynamic parameters, which can be tightly controlled and varied.

More specifically, our in vitro microvasculature also presents an experimental recapitulation of an ensemble of physiological processes, including platelet, leukocyte, and endothelial activation, adhesion molecule expression, cell aggregation, cytokine production, and interactions among these many different cell types as well as biophysical and rheological interactions among hemodynamics, microvascular geometry, and multiple cell types. Therefore, our microsystem is ideally suited for studying hematologic diseases involving microvascular occlusion and thrombosis in which interplay among those processes affects pathophysiology.

In this system, those pathophysiologic processes are collectively quantified in terms of flow velocity. Combining that data with data from standard methodologies, such as parallel plate flow chambers or micropipette aspiration, will enable the creation of a more comprehensive biophysical picture of microvascular occlusion and thrombosis, and this is a topic of ongoing work in our laboratory. With sickle cell vasoocclusion and HUS as prototypical disease targets, we demonstrated the utility and versatility of this system by conducting key clinically relevant biophysical experiments that are amenable to standard techniques. Furthermore, our pilot data establish the microvasculature on a chip as a viable drug discovery platform for assessing pharmacologic agents that affect microvascular flow or rheology.

Using SCD patient blood samples in our system clearly establishes the clinical utility of our microvasculature on a chip for studying hemodynamic questions related to the microvascular aspects of SCD or any other pathological condition involving microcirculatory obstruction. Furthermore, our data demonstrate the capabilities of our system in evaluating medications, such as HU, that affect biophysical properties of blood cells and microvascular blood flow in SCD.

In addition, our data using STX2-activated endothelial cells demonstrate the efficacy of our in vitro microvasculature model both as a system to study the biophysical aspects of microvascular thrombosis in diseases such as HUS and as a drug discovery platform for those disorders. The shear dependence of thrombi formation and microchannel obstruction we observed may be clinically relevant, as HUS usually occurs days after symptoms of the inciting infection present. STX2-induced thrombi may initially develop slowly with the narrowing of the lumen size in affected vessels potentially leading to increasing shear and establishing a vicious cycle of positive feedback that ultimately leads to microvascular obstruction.

As with other systems reported in the literature, use of microfluidics for conducting biomedical experiments conveys key advantages. Microfluidic systems are transparent and therefore easily adaptable to brightfield and fluorescence microscopy, allowing for the detection of specific biomolecules and cellular subpopulations of interest. Microscopy as a readout also enables straightforward quantitative analysis, which is essential for the investigation of biophysical phenomena. Furthermore, the ability to create any arbitrary pattern using standard microfabrication techniques provides the user with limitless design options. Indeed, with further development of this technology, a "multiplexed" microvasculature on a chip, capable of testing multiple endothelial cell types, drugs, cytokines, and shear rates simultaneously using a single sample of a patient's blood, can be created.

No in vitro device can fully recapitulate all in vivo conditions, and our system is not without limitations. For instance, our microfluidic channels are square in cross section. Although technically circular microchannels can be fabricated (15, 16), we opted to use a more simplified and standard fabrication procedure to allow other researchers to readily apply this system to their own work. In addition, the presence of the cultured endothelial cells naturally "rounds out" the effective lumen, enabling the system to be more physiologic. Furthermore, our fluid dynamic modeling reveals that the flow conditions in our system are comparable to those in the in vivo microvasculature. Finally, recent work characterizing blood flow in square and rectangular microchannels has shown that those geometries are suitable for blood rheology experiments (51).

The microvasculature on a chip reported here combines some of the key properties of the microvasculature in one device and in a manner amenable to sophisticated analysis. The reductionist approach of our system allows insight into the biophysical aspects of hematologic processes in isolation from confounders that may occur in vivo. Therefore, our microdevice complements in vivo models of disease and, due to its simplicity in preparation and use, can be used to inform and design in vivo experiments. Overall, the capability of the microvasculature on a chip to effectively recapitulate multiple types of cellular interactions under tightly controlled physiologic microcirculatory flow parameters will provide new biophysical insight into hematologic processes involving microvascular occlusion and thrombosis. By altering the design geometry and the cell type used to culture the inner surface of the microdevice, the system can also be modified to study biophysical or biotransport phenomena relevant in different anatomic sites or pathologic conditions. Examples would include culturing epithelial cells in the system for studying bacterial infections in a small airway model or culturing osteoblasts as a bone marrow microenvironment model to study hematopoietic stem cell interactions under flow. As a result, this system provides ample opportunities to apply the benefits of microfluidic technology to investigating clinically relevant biophysical questions.

Methods

Microdevice fabrication. The microfluidic device, designed in autoCAD to emulate physiologic postcapillary venule anatomy, was fabricated using both standard photolithography and soft lithography. With SU-8 Photoresist (MicroChem Inc.), the channel design was transferred to 6-inch silicon wafers. PDMS mixed at a 10:1 ratio (w/w) of polymer to curing agent was then poured onto the wafers and cured at 60°C for about 24 hours, after treating the wafers to prevent permanent PDMS adhesion. The cured device was then removed from the wafer, and holes were cored for the inlet, outlet, and bypass with a 1.5-mm hole puncher. The device and a thin sheet of PDMS, to be bonded as the bottom portion of the device, were then treated with tape and sonicated in ethanol for 10–15 minutes. The PDMS pieces were then rinsed thoroughly with deionized water and set to dry at 60°C in an oven. See Supplemental Information for more details.

Culturing endothelial cells in microdevice. In preparation for cell seeding, the top and bottom portions of the device were bonded via exposure to oxygen plasma (Plasmod) and the channels coated with 50 μg/ml fibronectin from human plasma (Sigma-Aldrich), incubating at 37°C, 5% CO_2 for 45–60 minutes. The channels were then rinsed with PBS. Cells were prepared at 500,000–3,000,000 cells/ml medium with 8% mass/volume dextran 500 (Sigma-Aldrich) and infused into the device at 1.25 μl/min for 2 hours with a syringe pump. Dextran increases the viscosity of the cell-seeding medium and decreases the velocity of endothelial cells as they enter the microfluidic system, which in turn increases the likelihood that the cells will adhere and culture. Afterwards, the cell suspension was replaced by fresh medium, which was then perfused through the device for 2–3 days at the same rate. See Supplemental Information for more details.

Fluid dynamics simulations and modeling. Computational simulations were made to assess the detailed flow characteristics in the smallest channels of the experimental microvasculature system. Confocal imaging, capable of resolving cytoplasmic and nuclear features of the endothelium, guided the construction of a computational model of a representative channel. Using elastic moduli taken from the literature, a 2D FSI simulation was performed on the multicomponent computational mesh to explore the extent of cellular deformation. Inlet flow was prescribed to give a centerline velocity of 1 mm/s, and outlet pressures were set at 0 pascals (Pa) to match experimental conditions. The Young's moduli of the endothelial cytoplasm and nuclei ($E_{cytoplasm}$ = 8.2 kPa, $E_{nucleus}$ = 15.1 kPa) were used to define nearly incompressible neo-Hookean material descriptions ($K_{cytoplasm}$ =137 kPa, $C_{cytoplasm}$ = 1.37 kPa; $K_{nucleus}$ = 252 kPa, $C_{nucleus}$ = 2.52 kPa) capable of large deformation (54), while the PDMS channel was assigned a Young's modulus of 500 kPa (55). Whole blood was a assigned a viscosity of 2.7 cP, a value experimentally reported for blood at the relevant shear stress in a tube with a diameter of 20–30 μm (56). The FSI model was solved using ADINA 8.5 (ADINA R&D), a well-validated commercial finite element solver suite commonly used for such simulations. Results of the FSI simulation demonstrated minimal cellular deformation (~2 nm) due to flow-induced shear stresses (~5 dyne/cm^2) under experimental flow conditions, in qualitative agreement with the time-dependent deformation observed for cells under similar shear (57). Given the vanishingly small effects of cellular deformation on the flow field and the substantial computational cost of FSI analysis, the remaining 3D simulations of different flow conditions were of the fluid domain only and were conducted in the well-validated finite volume Navier-Stokes solver FLUENT 12.0 (ANSYS; Supplemental Figure 3).

Human blood samples. Blood was collected in heparinized tubes (or EDTA tubes when compared with samples taken from SCD patients) from healthy volunteers after informed consent was obtained. For experiments related to SCD, blood was collected in EDTA tubes from patients diagnosed with hemoglobin SS known to be either receiving HU or not.

Microscopy and experimental setup. For spinning disc confocal imaging, an Axio Observer Z1 microscope (Carl Zeiss) with a laser-scanning confocal head (Yokogawa) was used, with image acquisition performed by a Cascade II:512 EMCCD camera (Photometrics). For the widefield imaging modes of epifluorescence and brightfield microscopy, the same Axio Observer Z1 microscopy base was used, with image acquisition performed by a CoolSnap CCD camera (Photometrics). The microscopy system, data acquisition, and analysis were managed through Metamorph Imaging Software (Molecular Devices). The endothelialized microdevices attached to a standard syringe pump (Harvard Apparatus) were transferred from a standard cell culture to a heated stage set at 37°C at the microscope.

Each microdevice was designed to accommodate the constant flow rate with a large outlet channel that bypassed the network of smallest channels to maintain a relatively constant pressure even when the majority of the channels were occluded (see Supplemental Information). As the blood or cell suspension left the syringe pump, the majority of the flow was directed into this bypass outlet, whereas the minority of flow entered the microfluidic channels to be assayed. Therefore, the obstruction of individual microchannels would have little effect on the pressure and flow in the other microchannels of the system.

Under the control conditions of each experiment described, whole blood mixed with 0.5-μm fluorescent beads (Invitrogen) was flowed into the device and tracked with epifluorescence videomicroscopy. To determine the appropriate pump settings, the flow rate was adjusted with the bypass channel open, so that beads flowing in the centerline of the smallest microchannels were consistently measured to maintain centerline velocities, V_{max}, appropriate for the physiologic condition. This pump setting, and therefore the initial shear stress, was then used for the other conditions of the same experiment, and bead tracking was used to determine the changes in centerline velocity due to adhesion or obstruction (Supplemental Video 15).

Anti–VE-cadherin staining. Use of anti–VE-cadherin–FITC (Cell Signaling Inc.) required an immunofluorescence protocol in which cells were fixed and permeabilized within the microfluidic system. Final dilutions of 1:200 to 1:100 of antibody were used.

Other dyes, reagents, and drugs. For confocal experiments, CellMask Orange (Invitrogen) and Syto-13 (Invitrogen) were used to label endothelial cell membrane and nuclei, respectively. DAF-2DA (EMD Chemicals) was used per manufacturer's specifications to measure NO. To label leukocytes and platelets, 1 μg/ml of R6G (Sigma-Aldrich) was added to whole blood. STX2 was purchased from Toxin Technology, and eptifibatide was a gift from Gillian Stephens (Portola Pharmaceuticals Inc).

Statistics. All reported microchannel velocity values represent the average centerline velocity, V_{max}, of 32 microchannels. Velocities were compared using Mann-Whitney analysis. Statistical significance was defined as $P < 0.05$.

Study approval. For all subjects, informed consent was obtained. All protocols were approved by the institutional review boards of the University of California, Berkeley, UCSF, and Emory University, where these studies were conducted.

Acknowledgments

We thank T. Hunt, M. Rosenbluth, D. Myers, Y. Sakurai, the rest of the Fletcher Lab, and the rest of the Lam Lab for their advice and useful discussions. Financial support for this work was provided by an NIH grant (K08-HL093360), a UCSF REAC award, an NIH Nanomedicine Development Center award (PN2EY018244), and funding from the Center for Endothelial Cell Biology of Children's Healthcare of Atlanta (to W.A. Lam), and an NSF CAREER award and NIH R01 grants to D.A. Fletcher.

Received for publication April 27, 2011, and accepted in revised form November 2, 2011.

Address correspondence to: Wilbur A. Lam, 2015 Uppergate Drive NE, Emory Children's Center — Room 412, Atlanta, Georgia 30030, USA. Phone: 415.385.3446; Fax: 404.727.4455; E-mail: wilbur.lam@emory.edu.

1. Ballas SK, Mohandas N. Sickle red cell microrheology and sickle blood rheology. *Microcirculation*. 2004;11(2):209–225.
2. Bunn HF. Pathogenesis and treatment of sickle cell disease. *N Engl J Med*. 1997;337(11):762–769.
3. Moake JL. Thrombotic microangiopathies. *N Engl J Med*. 2002;347(8):589–600.
4. Lipowsky HH. Microvascular rheology and hemodynamics. *Microcirculation*. 2005;12(1):5–15.
5. Barabino GA, Platt MO, Kaul DK. Sickle cell biomechanics. *Annu Rev Biomed Eng*. 2010;12:345–367.
6. Bao G, Suresh S. Cell and molecular mechanics of biological materials. *Nat Mater*. 2003;2(11):715–725.
7. Kaul DK, Finnegan E, Barabino GA. Sickle red cell-endothelium interactions. *Microcirculation*. 2009;16(1):97–111.
8. Mezzano D, Quiroga T, Pereira J. The level of laboratory testing required for diagnosis or exclusion of a platelet function disorder using platelet aggregation and secretion assays. *Semin Thromb Hemost*. 2009;35(2):242–254.
9. Young EW, Beebe DJ. Fundamentals of microfluidic cell culture in controlled microenvironments. *Chem Soc Rev*. 2010;39(3):1036–1048.
10. Young EW, Simmons CA. Macro- and microscale fluid flow systems for endothelial cell biology. *Lab Chip*. 2010;10(2):143–160.
11. Higgins JM, Eddington DT, Bhatia SN, Mahadevan L. Sickle cell vasoocclusion and rescue in a microfluidic device. *Proc Natl Acad Sci U S A*. 2007;104(51):20496–20500.
12. Rosano JM, et al. A physiologically realistic in vitro model of microvascular networks. *Biomed Microdevices*. 2009;11(5):1051–1057.
13. Kotz KT, et al. Clinical microfluidics for neutrophil genomics and proteomics. *Nat Med*. 2010;16(9):1042–1047.
14. Rosenbluth MJ, Lam WA, Fletcher DA. Analyzing cell mechanics in hematologic diseases with microfluidic biophysical flow cytometry. *Lab Chip*. 2008;8(7):1062–1070.
15. Shelby JP, White J, Ganesan K, Rathod PK, Chiu DT. A microfluidic model for single-cell capillary obstruction by Plasmodium falciparum-infected erythrocytes. *Proc Natl Acad Sci U S A*. 2003;100(25):14618–14622.
16. Borenstein JT, et al. Functional endothelialized microvascular networks with circular cross-sections in a tissue culture substrate. *Biomed Microdevices*. 2010;12(1):71–79.
17. Nesbitt WS, et al. A shear gradient-dependent platelet aggregation mechanism drives thrombus formation. *Nat Med*. 2009;15(6):665–673.
18. Fiddes LK, et al. A circular cross-section PDMS microfluidics system for replication of cardiovascular flow conditions. *Biomaterials*. 2010;31(13):3459–3464.
19. Lee SH, Kang do H, Kim HN, Suh KY. Use of directly molded poly(methyl methacrylate) channels for microfluidic applications. *Lab Chip*. 2010;10(23):3300–3306.
20. Michel T, Vanhoutte PM. Cellular signaling and NO production. *Pflugers Arch*. 2010;459(6):807–816.
21. Qiu W, Kass DA, Hu Q, Ziegelstein RC. Determinants of shear stress-stimulated endothelial nitric oxide production assessed in real-time by 4,5-diaminofluorescein fluorescence. *Biochem Biophys Res Commun*. 2001;286(2):328–335.
22. Vestweber D. VE-cadherin: the major endothelial adhesion molecule controlling cellular junctions and blood vessel formation. *Arterioscler Thromb Vasc Biol*. 2008;28(2):223–232.
23. Pries AR, Secomb TW, Gessner T, Sperandio MB, Gross JF, Gaehtgens P. Resistance to blood flow in microvessels in vivo. *Circ Res*. 1994;75(5):904–915.
24. Fung YC. *Biomechanics: Circulation*. 2nd ed. New York, New York, USA: Springer Publishing; 1997.
25. Ruggeri ZM, Mendolicchio GL. Adhesion mechanisms in platelet function. *Circ Res*. 2007; 100(12):1673–1685.
26. Granger DN, Kubes P. The microcirculation and inflammation: modulation of leukocyte-endothelial cell adhesion. *J Leukoc Biol*. 1994;55(5):662–675.
27. Perry MA, Granger DN. Role of CD11/CD18 in shear rate-dependent leukocyte-endothelial cell interactions in cat mesenteric venules. *J Clin Invest*. 1991;87(5):1798–1804.
28. Ishikawa M, et al. Platelet adhesion and arteriolar dilation in the photothrombosis: observation with the rat closed cranial and spinal windows. *J Neurol Sci*. 2002;194(1):59–69.
29. Dirnagl U, Niwa K, Sixt G, Villringer A. Cortical hypoperfusion after global forebrain ischemia in rats is not caused by microvascular leukocyte plugging. *Stroke*. 1994;25(5):1028–1038.
30. Sluiter W, Pietersma A, Lamers JM, Koster JF. Leukocyte adhesion molecules on the vascular endothelium: their role in the pathogenesis of cardiovascular disease and the mechanisms underlying their expression. *J Cardiovasc Pharmacol*. 1993;22(suppl 4):S37–S44.
31. Pathare A, Kindi SA, Daar S, Dennison D. Cytokines in sickle cell disease. *Hematology*. 2003;8(5):329–337.
32. Lucas R, Lou J, Morel DR, Ricou B, Suter PM, Grau GE. TNF receptors in the microvascular pathology of acute respiratory distress syndrome and cerebral malaria. *J Leukoc Biol*. 1997;61(5):551–558.
33. Worthen GS, Schwab B 3rd, Elson EL, Downey GP. Mechanics of stimulated neutrophils: cell stiffening induces retention in capillaries. *Science*. 1989;245(4914):183–186.
34. Nash GB, Johnson CS, Meiselman HJ. Rheologic impairment of sickle RBCs induced by repetitive cycles of deoxygenation-reoxygenation. *Blood*. 1988;72(2):539–545.
35. Mohandas N, Evans E. Sickle erythrocyte adherence to vascular endothelium. Morphologic correlates and the requirement for divalent cations and collagen-binding plasma proteins. *J Clin Invest*. 1985;76(4):1605–1612.
36. Barabino GA, McIntire LV, Eskin SG, Sears DA, Udden M. Endothelial cell interactions with sickle cell, sickle trait, mechanically injured, and normal erythrocytes under controlled flow. *Blood*. 1987;70(1):152–157.

37. Ware RE. How I use hydroxyurea to treat young patients with sickle cell anemia. *Blood*. 2010; 115(26):5300–5311.
38. Athanassiou G, Moutzouri A, Kourakli A, Zoumbos N. Effect of hydroxyurea on the deformability of the red blood cell membrane in patients with sickle cell anemia. *Clin Hemorheol Microcirc*. 2006;35(1–2):291–295.
39. Brandao MM, et al. Optical tweezers for measuring red blood cell elasticity: application to the study of drug response in sickle cell disease. *Eur J Haematol*. 2003;70(4):207–211.
40. Bridges KR, et al. A multiparameter analysis of sickle erythrocytes in patients undergoing hydroxyurea therapy. *Blood*. 1996;88(12):4701–4710.
41. Ware RE, Aygun B. Advances in the use of hydroxyurea. *Hematology Am Soc Hematol Educ Program*. 2009:62–69.
42. Gladwin MT, et al. Nitric oxide donor properties of hydroxyurea in patients with sickle cell disease. *Br J Haematol*. 2002;116(2):436–444.
43. Ware RE, et al. Predictors of fetal hemoglobin response in children with sickle cell anemia receiving hydroxyurea therapy. *Blood*. 2002;99(1):10–14.
44. Verduzco LA, Nathan DG. Sickle cell disease and stroke. *Blood*. 2009;114(25):5117–5125.
45. Cheung AT, et al. Microvascular abnormalities in sickle cell disease: a computer-assisted intravital microscopy study. *Blood*. 2002;99(11):3999–4005.
46. Hidalgo A, Chang J, Jang JE, Peired AJ, Chiang EY, Frenette PS. Heterotypic interactions enabled by polarized neutrophil microdomains mediate thromboinflammatory injury. *Nat Med*. 2009;15(4):384–391.
47. Zoja C, Buelli S, Morigi M. Shiga toxin-associated hemolytic uremic syndrome: pathophysiology of endothelial dysfunction. *Pediatr Nephrol*. 2010;25(11):2231–2240.
48. Nolasco LH, et al. Hemolytic uremic syndrome-associated Shiga toxins promote endothelial-cell secretion and impair ADAMTS13 cleavage of unusually large von Willebrand factor multimers. *Blood*. 2005;106(13):4199–4209.
49. Morigi M, et al. Verotoxin-1-induced up-regulation of adhesive molecules renders microvascular endothelial cells thrombogenic at high shear stress. *Blood*. 2001;98(6):1828–1835.
50. Chau L, Doran M, Cooper-White J. A novel multi-shear microdevice for studying cell mechanics. *Lab Chip*. 2009;9(13):1897–1902.
51. Green DA, Murphy WG, Uttley WS. Haemolytic uraemic syndrome: prognostic factors. *Clin Lab Haematol*. 2000;22(1):11–14.
52. Walters MD, Matthei IU, Kay R, Dillon MJ, Barratt TM. The polymorphonuclear leucocyte count in childhood haemolytic uraemic syndrome. *Pediatr Nephrol*. 1989;3(2):130–134.
53. Curran MP, Keating GM. Eptifibatide: a review of its use in patients with acute coronary syndromes and/or undergoing percutaneous coronary intervention. *Drugs*. 2005;65(14):2009–2035.
54. Mathur AB, Reichert WM, Truskey GA. Flow and high affinity binding affect the elastic modulus of the nucleus, cell body and the stress fibers of endothelial cells. *Ann Biomed Eng*. 2007;35(7):1120–1130.
55. Armani D, Liu C, Aluru N. Re-configurable fluid circuits by PDMS elastomer micromachining. Presented at: Micro Electro Mechanical Systems, 1999. MEMS '99. Twelfth IEEE International Conference; January 17–21, 1999; Orlando, Florida, USA.
56. Reinke W, Gaehtgens P, Johnson PC. Blood viscosity in small tubes: effect of shear rate, aggregation, and sedimentation. *Am J Physiol*. 1987; 253(3 pt 2):H540–H547.
57. Dangaria JH, Butler PJ. Macrorheology and adaptive microrheology of endothelial cells subjected to fluid shear stress. *Am J Physiol Cell Physiol*. 2007;293(5):C1568–C1575.